Available online at www.sciencedirect.com
ScienceDirect
Journal of Photochemistry and Photobiology A: Chemistry 183 (2006) 22–30
Journal of Photochemistry and Photobiology A:Chemistry
www.elsevier.com/locate/jphotochem

Enhanced intersystem crossings of S_1–T_1 and T_1–S_0 in coronene– and pyrene–galvinoxyl systems as studied by a pulsed ESR method

Hajime Terazono, Akio Kawai, Kazuhide Tsuji [1], Kazuhiko Shibuya *

Department of Chemistry, Graduate School of Science and Engineering, Tokyo Institute of Technology, 2-12-1-H57 Ohokayama, Meguro-ku, Tokyo 152-8551, Japan

Received 26 December 2005; received in revised form 8 February 2006; accepted 9 February 2006
Available online 31 March 2006

Abstract

Radical enhanced intersystem crossing (EISC) of S_1–T_1 and T_1–S_0 in excited molecule–radical systems was investigated by observing chemically induced dynamic electron polarization of radicals with a time-resolved (TR) ESR method. Time profiles of CIDEP were observed in excited coronene–radical systems, where the radical was 2,2,6,6-tetramethyl-1-piperidinyloxyl (TEMPO), 2-phenyl-4,4,5,5-tetramethylimidazoline-3-oxide-1-oxyl (PTIO), 1,1-diphenyl-2-picrylhydrazyl (DPPH), 1,3,5-triphenylverdazyl (TPV) or galvinoxyl (Galv). In two systems containing TEMPO and PTIO radicals, signals due to the quenching of coronene in both S_1 and T_1 states were observed, while in other three systems containing DPPH, TPV, and Galv radicals only the signals induced by triplet coronene–radical pair interaction could be observed. To make the quantitative analysis on CIDEP created in S_1- and T_1-quenching processes, a pulsed ESR method was applied for a coronene–Galv system chosen as a model system. The absolute magnitude of CIDEP of Galv radical created by S_1- and T_1-quenching processes ($|P_n^{QP}|$ and $|P_n^{DP}|$, respectively) were determined to be $7P_{eq}$ and $0.8P_{eq}$, respectively, where P_{eq} is the equilibrium Boltzmann polarization at room temperature. According to the CIDEP theory, the large $|P_n^{QP}/P_n^{DP}|$ ratio of ca. 9 indicates that the S_1–T_1 EISC occurs through a long distance interaction which is mediated by intermolecular charge transfer state, while $|P_n^{QP}|$ of $7P_{eq}$ indicates T_1–S_0 enhanced ISC is promoted by exchange interaction at the nearly contact coronene–Galv pair. Another system of pyrene–Galv pair was also discussed to confirm the proposed interaction model for the enhanced ISC.

Keywords: Quenching; Enhanced intersystem crossing; CIDEP; Pulsed ESR

1. Introduction

Quenching of an electronically excited molecule is one of the most important and fundamental processes in photochemistry. Among various quenching pathways through electron interaction, electron transfer, energy transfer and so on, enhanced intersystem crossing (EISC) induced by paramagnetic species such as free radical and molecular oxygen is crucial to electronic relaxation and plays a central role in photochemistry. Since pioneering works on EISC reported by Porter and his coworkers [1], many EISC processes have been investigated on the basis of kinetic rate constants measured by optical techniques [2]. Nevertheless kinetic data do not provide microscopic information on exchange interaction to induce the EISC itself. It was then required to obtain experimental information to promote better understanding of the EISC processes.

In 1980s, the chemically induced dynamic electron polarization (CIDEP) creation accompanied by the EISC processes was found as another observable phenomenon [3]. The CIDEP signals were created on radicals through electron interaction between a triplet molecule and a doublet radical. The signal analysis, therefore, gave us further details about electronic quenching; intermolecular potentials of radical–triplet pairs, energy gaps between quartet and doublet states of radical–triplet pairs, signs of exchange interaction, and so on. Microscopic information became available from a viewpoint of electron spin dynamics.

Paul and coworkers assumed that zero field splitting interaction within a triplet (T_1) manifold causes the CIDEP [4]. Kawai et al. successfully explained that the CIDEP is induced by nonadiabatic transition along intermolecular potentials [5].

* Corresponding author. Tel.: +81 3 5734 2224; fax: +81 3 5734 2224.
E-mail address: kshibuya@chem.titech.ac.jp (K. Shibuya).
[1] Present address: Gunma National College of Technology, 580 Toriba-machi Maebashi, Gunma 371-8530, Japan.

1010-6030/$ – see front matter © 2006 Elsevier B.V. All rights reserved.
doi:10.1016/j.jphotochem.2006.02.014

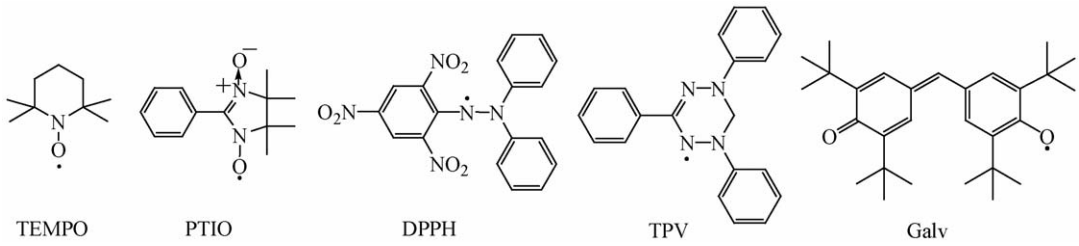

Fig. 1. Molecular structures of free radicals used in the present study and their abbreviations.

The CIDEP due to singlet (S_1)-quenching by a radical was also observed with the phase opposite to that due to T_1-quenching [6]. After these experimental findings, theoretical studies started as well [7,8]. Shushin formulated a stochastic Liouville equation on the basis of a diffusion model and derived formulas to determine absolute spin polarization [7].

In this paper, the CIDEP generated by quenching of photoexcited coronene in the S_1 and T_1 states was studied for five radicals shown in Fig. 1 to obtain the detailed information on a CIDEP creation mechanism or the enhanced intersystem crossing.

The present results obtained by a time-resolved (TR) ESR method are classified into two types of CIDEP signals: one due to T_1–S_0 EISC and the other due to both S_1–T_1 and T_1–S_0 EISCs. Relative CIDEP intensities due to S_1–T_1 and T_1–S_0 EISCs strongly depend on a radical employed. To make the quantitative analysis for a coronene–galvinoxyl (Galv) system, the CIDEP time profile was measured by a pulsed ESR method and kinetically simulated. Absolute spin polarization was determined and interpreted in terms of a theoretical model proposed by Shushin. The analysis suggests that the CIDEP due to S_1–T_1 EISC is created through a long distance interaction of coronene in the S_1 state and Galv radical. The present results for a coronene–Galv system are compared with those for a coronene–2,2,6,6-tetramethyl-1-piperidinyloxyl (TEMPO) system [9]. A pyrene–Galv system was also examined by a pulsed ESR method. A proposed quenching model is discussed.

2. Experimental

Coronene (Tokyo Kasei) and pyrene (Kanto Chemicals) were photoexcited to the S_1 and T_1 states. *Trans*-stilbene (Tokyo Kasei) was used as a triplet quencher. Toluene and anisole (Kanto Chemicals, GR-grade) were used as solvent. Four radicals of TEMPO, 2-phenyl-4,4,5,5-tetramethylimidazoline-3-oxide-1-oxyl (PTIO), 1,1-diphenyl-2-picrylhydrazyl (DPPH), and Galv were obtained from Tokyo Kasei. A 1,3,5-triphenylverdazyl (TPV) radical was synthesized according to the literature [10] and purified with column chromatography. The synthesized radical presented the CW-ESR [10] and optical absorption [11] spectra reported for TPV. Sample solutions, except for coronene–TPV solution degassed by freeze–pump–thaw cycles, were degassed by Ar and flowed through quartz cells. All experiments were performed at room temperature.

Pulsed ESR signals were detected by an X-band ESR spectrometer (Brucker Elexsys E580, 9.65 GHz). The microwave was pulsed by a pin-photodiode and enhanced by a traveling wave tube amplifier. Pulsed ESR signals were enhanced by a video amplifier and integrated by a digitizer. Pulsed ESR spectra were obtained by Fourier-transformation of free induction decay (FID). CIDEP time profiles were obtained by measuring FID intensities as a function of delay time between laser and pulsed MW irradiations. A phase cycling, CYCLOPS [12], was performed to remove artificial noise.

Transient TR-ESR signals generated by the pulsed laser irradiation were detected by a diode of a conventional X-band ESR spectrometer and were transferred to a boxcar integrator (Standard Research Systems SR-250) for measurements of TR-ESR spectra or a transient memory (Tektronix TDS 350) for ESR signal time profiles without magnetic field modulation (100 kHz). The width of the gate time of the boxcar integrator and microwave power were suitably set in each measurement. A homemade wide band amplifier (LH0032, 10 MHz) was used to improve S/N ratios.

A time-resolved thermal lensing method [13] was used to determine the quantum yield of S_1–T_1 EISC. A He–Ne laser (NEC GLG-5780) was used to monitor time-resolved thermal lensing signals. The monitoring light traveled approximately parallel to an excitation light (355 nm) through a sample cell, was detected by a photomultiplier tube (Hamamatsu R928), and was measured with a transient memory (Tektronix TDS620B).

Time-resolved fluorescence was measured to determine fluorescence lifetimes and fluorescence quenching rate constants. The experimental setup was essentially the same as that used in the previous papers [9,14].

The third harmonics (355 nm) of a nanosecond Nd^{3+}:YAG laser (Continuum Powerlight 8000, 10 Hz for ESR and time-resolved fluorescence methods/Continuum Surelight I-10, 1 Hz for a time-resolved thermal lensing method) was used for an excitation light source except for a coronene–PTIO system. The 297 nm light was used for an excitation light source in a coronene–PTIO system. The laser powers were 0.5–12 mJ/pulse for ESR and time-resolved fluorescence methods, and attenuated for a time-resolved thermal lensing method. Initial concentrations of excited molecules were on the order of 10^{-5} M (M = mol/dm^3). A quartz columnar cell with 3.0 mm diameter, a quartz flat cell with 0.5 mm width and a quartz rectangular cell with 10 mm width were used for ESR, time-resolved fluorescence, and time-resolved thermal lensing methods, respectively.

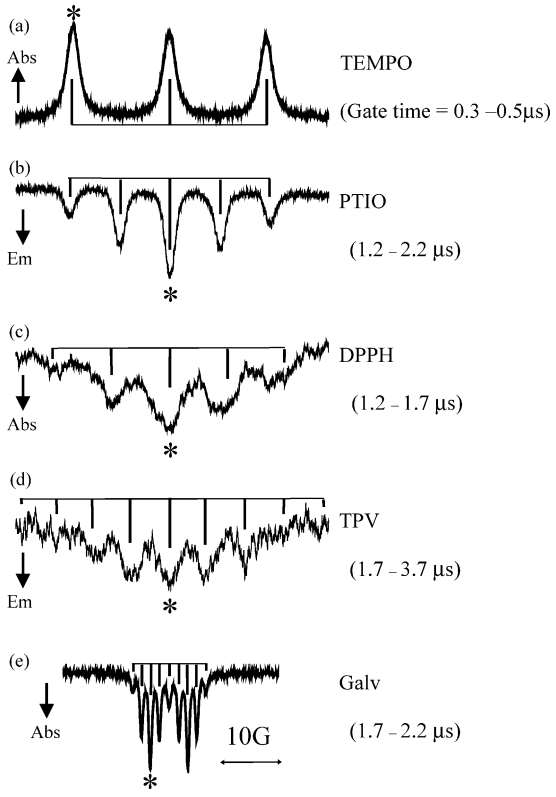

Fig. 2. TR-ESR spectra of coronene (2.0 mM)–radical systems. (a) TEMPO (3.5 mM), (b) PTIO (0.50 mM), (c) DPPH (0.29 mM), (d) TPV (1.0 mM), and (e) Galv (0.10 mM). Samples were dissolved in toluene except (d) TPV dissolved in anisole.

3. Results and discussion

3.1. CIDEP signals generated through electronic quenching by various radicals

Fig. 2 shows the TR-ESR spectra obtained by a UV laser excitation of coronene–radical systems, where the radical is (a) TEMPO, (b) PTIO, (c) DPPH, (d) TPV, or (e) Galv. In each system, the hyperfine structure exactly coincides with the pattern predicted for the corresponding radical and the continuous wave ESR (CW-MW ESR) spectrum, which suggests that a spin-polarized signal is created on the radical of interest.

Fig. 3 shows the CIDEP time profiles obtained in these coronene–radical systems.

According to previous studies [9], the CIDEP time profile in a coronene–TEMPO system contains two opposite phase signals due to (1) S_1–radical encounter in an earlier time region and (2) T_1–radical encounter in a later time region. In Fig. 3, upward and downward components correspond to CIDEP signals created by the radical quenching of coronene in the S_1 state (S_1-quenching) and the quenching of coronene in the T_1 state (T_1-quenching). The CIDEP signal due to T_1-quenching was easily assigned, because it was quenched in the presence of triplet quencher such as molecular oxygen or *trans*-stilbene.

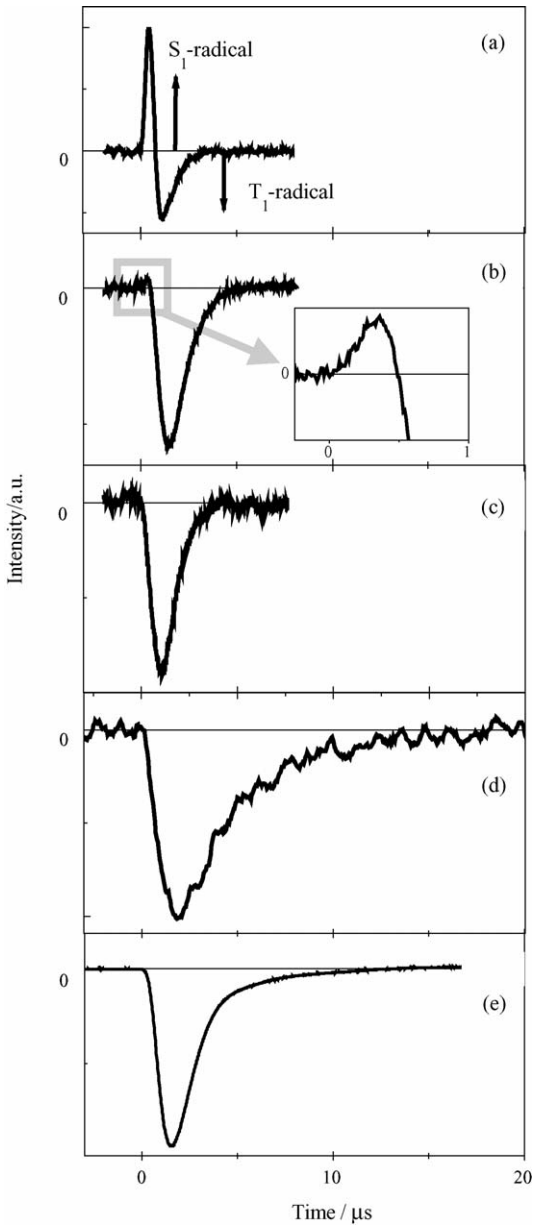

Fig. 3. Time profiles of TR-ESR signal due to electronic quenching of photoexcited coronene by various radicals. Upward and downward components indicate signals due to S_1–radical and T_1–radical systems, respectively. The applied magnetic fields were fixed at the peaks with asterisk (∗) in Fig. 2. (a) Coronene–TEMPO, (b) coronene–PTIO, (c) coronene–DPPH, (d) coronene–TPV, and (e) coronene–Galv.

All the relaxation processes and rate constants related to the present quenching processes are described below:

$$S_1 \xrightarrow{k_f+k_{IC}} S_0, \quad \text{fluorescence and internal conversion (IC)} \tag{1}$$

$$S_1 \xrightarrow{k_{ISC}} T_1, \quad \text{intersystem crossing (ISC)} \tag{2}$$

$$S_1 + R \xrightarrow{k_{EIC}} S_0 + R, \quad \text{enhanced IC} \tag{3}$$

$$S_1 + R \xrightarrow{k_{EISC}} T_1 + R^{\#}, \quad \text{EISC} \tag{4}$$

$$T_1 \xrightarrow{k_0^T} S_0, \quad \text{ISC} \tag{5}$$

$$T_1 + R \xrightarrow{k_q^T} S_0 + R^{\#\#}, \quad \text{EISC} \tag{6}$$

The S_1 molecule produced by laser irradiation relaxes through process 1 (fluorescence and S_1–S_0 IC), process 2 (S_1–T_1 ISC), process 3 (S_1–S_0 enhanced IC), and process 4 (S_1–T_1 EISC). The T_1 molecule relaxes through process 5 (T_1–S_0 ISC) and process 6 (T_1–S_0 EISC or T_1-quenching). The CIDEP signals are created on radical through processes 4 and 6. The symbols, $R^{\#}$ and $R^{\#\#}$, stand for spin-polarized radicals generated by processes 4 and 6, respectively. The spin-polarized $R^{\#}$ and $R^{\#\#}$ have opposite phases of CIDEP. Since $R^{\#}$ is generated through S_1-quenching process, the $R^{\#}$ signal appears earlier than the $R^{\#\#}$ signal generated through T_1-quenching. Fig. 3a of coronene–TEMPO system shows a good example of this type spin polarization generation. The TR-ESR signal of TEMPO starts with the positive signal due to the S_1–radical encounter until 1 μs, and then the negative signal due to the T_1–radical encounter appears after 1 μs.

Similar feature was observed in a coronene–PTIO system as shown in the inset of Fig. 3b for an enlarged view near $t = 0$ μs, though the CIDEP signal due to $R^{\#}$ became extremely weak. Unfortunately, no clear $R^{\#}$ signals due to S_1-quenching process were seen in other coronene–radical systems as seen in (c) a coronene–DPPH, (d) a coronene–TPV, and (e) a coronene–Galv, where only the CIDEP signals due to $R^{\#\#}$ were observed. To observe clear $R^{\#}$ signals due to S_1-quenching in these systems, one of the experimental procedure is to increase radical concentration. However, PTIO, DPPH, TPV, and Galv have strong light absorption bands and selective photoexcitation of coronene becomes difficult when the concentrations of these radicals increase. We consider that the CIDEP intensity is related to the nature of quenching processes, and more quantitative analysis will give us some unique information on both S_1- and T_1-quenching processes. Therefore, we will evaluate the absolute magnitudes of CIDEP in both S_1- and T_1-quenching processes and their creation mechanisms by analyzing the CIDEP time profiles measured accurately by pulsed-ESR technique on the basis of kinetic constants governing these photochemical systems.

3.2. Quantitative analysis by pulsed ESR

A CIDEP time profile was obtained with a pulsed ESR method. Magnetization along z-axis consisting of CIDEP and equilibrium Boltzmann polarization was turned to xy-plane. The FID intensities were measured as a function of delay time (t) with a pulse sequence: laser pulse–t–$\pi/2$ MW pulse–FID detection. Fig. 4 shows a CIDEP time profile (a) of TEMPO measured by a pulsed ESR method, together with a time profile (c) of TEMPO monitored by a TR-ESR method.

A pulsed ESR signal was normalized by the signal intensity due to thermal magnetization of TEMPO. As described for the explanation of Fig. 3, the upward and downward components mean signal intensities due to $R^{\#}$ and $R^{\#\#}$ generated by processes (4) and (6), respectively. The fast rise due to the S_1–radical interaction appears in an early time region and then the T_1–radical interaction appears in a later time region.

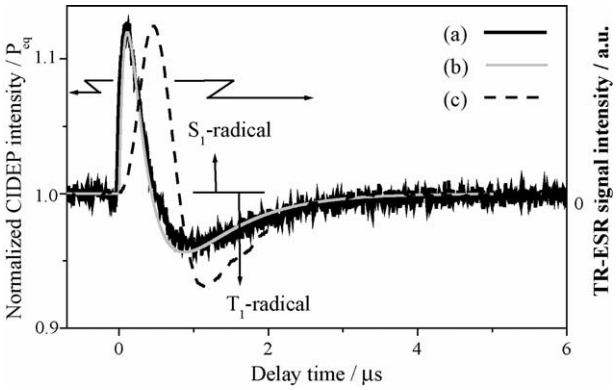

Fig. 4. Time profiles of TEMPO signal in a coronene–TEMPO system in anisole. (a) Pulsed ESR (experiment), (b) pulsed ESR (simulation), and (c) TR-ESR (experiment, the same as Fig. 2a).

The time profile (a) is simulated by the following three equations:

$$\frac{dM_z}{dt} = -\frac{(M_z - P_{eq}[R])}{T_1^R} + |P_n^{DP}|k_q^S f_T[R][S_1] - |P_n^{QP}|k_q^T[R][T_1] \tag{7}$$

$$\frac{d[S_1]}{dt} = -(k_0^S + k_q^S[R])[S_1] \tag{8}$$

$$\frac{d[T_1]}{dt} = (k_{ISC} + k_{EISC}[R])[S_1] - (k_0^T + k_q^T[R])[T_1] \tag{9}$$

where M_z is magnetization along z-axis. T_1^R is spin-lattice relaxation time of a radical. $|P_n^{DP}|$ and $|P_n^{QP}|$ are absolute magnitudes of CIDEP, spin polarizations, due to S_1–radical and T_1–radical systems, respectively. P_{eq} is equilibrium Boltzmann polarization. $[S_1]$, $[T_1]$, and $[R]$ are the concentrations of S_1, T_1, and radical.

Using kinetic constants reported [9], we simulated the time profile with two parameters, $|P_n^{DP}|$ and $|P_n^{QP}|$. The experimental time profile (a) is well reproduced by the simulation (b) where $|P_n^{DP}|$ and $|P_n^{QP}|$ values are $1.8P_{eq}$ and $2.2P_{eq}$, respectively. Table 1 lists these values and $|P_n^{QP}/P_n^{DP}|$ ratio, which will be discussed later.

These values agree well with previous results obtained from a traditional TR-ESR method [9]. Reliable $|P_n^{QP}|$ and $|P_n^{DP}|$ values were obtained from much simpler analysis based on the present pulsed ESR experiment. Thus, the pulsed ESR method is confirmed to be useful for the analysis of CIDEP created in excited molecule–radical systems.

Two types of CIDEP time profiles were created in coronene–radical systems. In (a) coronene–TEMPO and (b) coronene–PTIO systems, the CIDEP signals due to both

Table 1
Spin polarizations, $|P_n^{QP}|$ and $|P_n^{DP}|$ in a coronene–TEMPO system in anisole

$\lvert P_n^{QP}\rvert$	$\lvert P_n^{DP}\rvert$	$\lvert P_n^{QP}/P_n^{DP}\rvert$
$2.2P_{eq}$	$1.8P_{eq}$	1.2

S_1–radical and T_1–radical encounters were obtained. In (c) coronene–DPPH, (d) coronene–TPV, and (e) coronene–Galv systems, the CIDEP signals due to only T_1–radical encounter were obtained. To discuss the details of the electronic quenching processes, we decided to compare quantitatively two extreme cases of (a) coronene–TEMPO and (e) coronene–Galv systems. The former (a) system was already investigated and we know the experimental results [9]. In the present study, the coronene–Galv system was examined by a pulsed ESR method and the results were compared with the previous results for coronene–TEMPO. Furthermore, another pyrene–Galv system was examined in addition to the coronene–Galv system, because CIDEP time profile in a pyrene–radical system also depends on radical: both CIDEP due to S_1– and T_1–radical encounters were observed in pyrene–TEMPO and –PTIO systems while CIDEP of only T_1–radical encounter were seen in pyrene–DPPH, –TPV, and –Galv systems.

3.3. Pulsed ESR measurement of CIDEP in coronene– and pyrene–Galv systems

Fig. 5b shows Fourier-transformed spectrum of Galv, which was obtained from the FID presented in Fig. 5a.

As the hyperfine structure corresponds to CW-ESR spectrum of Galv, the spectral carrier responsible for Fig. 5b is Galv without doubt. Spectral feature of Fourier-transformation spectrum measured at various delay times from 1.0 to 2.5 μs was all the same, which implies that we measured the CIDEP of Galv and nothing else at any delay time in the coronene–Galv system. It should be mentioned here that we also observed the same of Galv spectra in a pyrene–Galv system as in the above coronene–Galv system.

3.4. Determination of kinetic constants

Before we analyze the CIDEP time profile created in coronene– and pyrene–Galv systems, it is necessary to determine various kinetic constants in Eqs. (7)–(9). The k_0^S (=$k_f + k_{IC}$) and k_q^S (=$k_{EIC} + k_{EISC}$) values were obtained to be $8.1 \times 10^6\ s^{-1}$ and $1.45 \times 10^{10}\ M^{-1}\ s^{-1}$ for a coronene–Galv system, and $16 \times 10^6\ s^{-1}$ and $6.4 \times 10^{10}\ M^{-1}\ s^{-1}$ for a pyrene–Galv system by a time-resolved fluorescence method and from a Stern–Volmer analysis, respectively. The k_{EISC} value for a coronene–Galv system was derived to be $9.9 \times 10^9\ M^{-1}\ s^{-1}$ from a time-resolved thermal lensing method according to the procedure described previously [9]. A fraction (f_T) of S_1–T_1 EISC in S_1-quenching for a coronene–Galv system is determined to be 0.68 by:

$$f_T = \frac{k_{EISC}}{k_q^S} \tag{10}$$

It might be worthy of note that the f_T value of 0.68 for a coronene–Galv system is comparable to 0.71 for a coronene–TEMPO system. Nevertheless, we observed strong CIDEP in an S_1 coronene–TEMPO system but negligibly weak

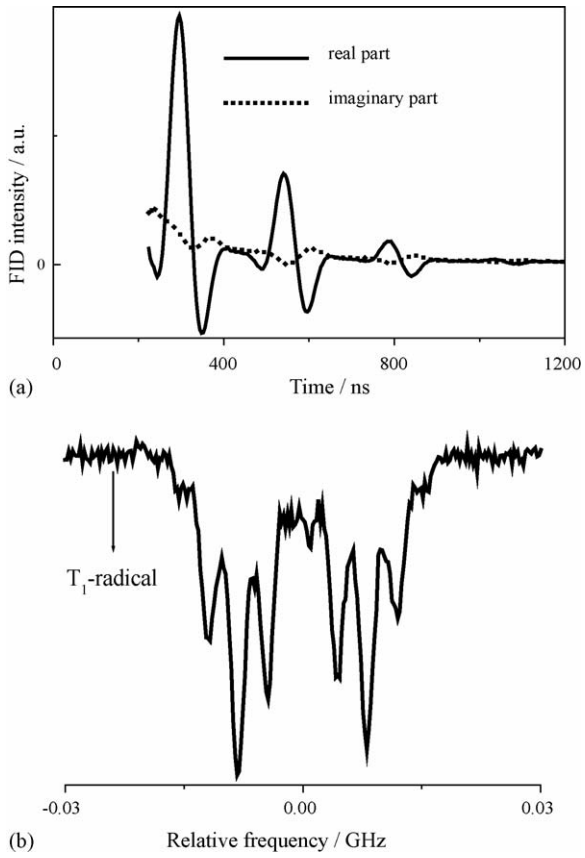

Fig. 5. Free induction decay (FID) and the Fourier transformed ESR spectrum. (a) Real and imaginary parts of FID of Galv. The $\pi/2$ MW pulse was irradiated at 1.4 μs after laser irradiation. (b) FT-ESR spectrum of Galv. A coronene (2.0 mM)–Galv (0.10 mM) systems in toluene was used.

Table 2
Kinetic constants used for analysis in coronene–Galv and pyrene–Galv systems in toluene

	k_0^S (s^{-1})[a]	k_{ISC} (s^{-1})[b]	k_0^T (s^{-1})[c]	k_q^S ($M^{-1}\ s^{-1}$)[a]	k_{EISC} ($M^{-1}\ s^{-1}$)	k_q^T ($M^{-1}\ s^{-1}$)[c]	T_1^R(μs)[d]
Coronene–Galv	8.1×10^6	5.2×10^6	6.0×10^5	1.45×10^{10}	9.9×10^9	5.4×10^9	2.2
Pyrene–Galv	16×10^6	5.9×10^6	2.5×10^5	6.4×10^{9}[e]	6.4×10^{9}[f]	4.7×10^9	2.2

[a] Determined by a fluorescence method.
[b] The values were calculated by using $\Phi_{ISC} = 0.64$ (coronene–Galv) [9] and 0.37 (pyrene–Galv) [15] as follows: $k_{ISC} = k_0^S \times \Phi_{ISC}$.
[c] Determined by a transient absorption method [16].
[d] Determined by an inversion recovery method.
[e] Since the reference value was measured in *n*-hexane, we corrected the value by considering viscosity of solvent as $k_q^S(\text{toluene}) = k_q^S(\text{hexane}) \times \frac{\eta(\text{hexane})}{\eta(\text{toluene})} = 1.2 \times 10^{10}\ M^{-1}\ s^{-1}$ [17] × 0.294 mPa s/0.553 mPa s [9].
[f] The f_T value is assumed as 1.0.

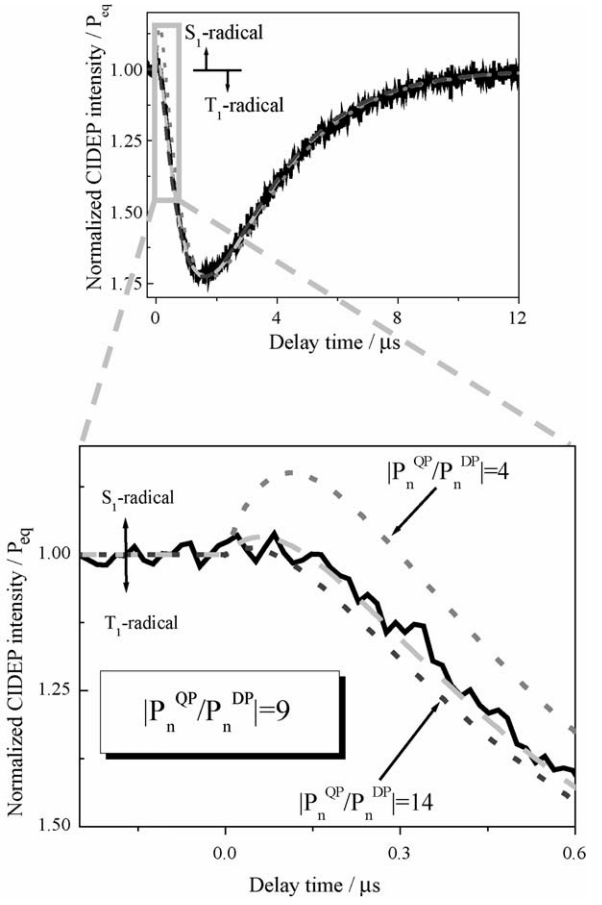

Fig. 6. Time profile of Galv signal in a coronene (2.0 mM)–Galv (0.077 mM) system in toluene. The simulation (broken lines) was carried out for the best fit at $|P_n^{QP}/P_n^{DP}| = 9$, together with the results for $|P_n^{QP}/P_n^{DP}| = 4$ and 14.

signal in an S_1 coronene–Galv system as seen in Fig. 3e. A T_1^R value for a Galv radical was determined to be 2.2 μs by an inversion recovery method. All the experimental values are summarized in Table 2, together with the data necessary for a pyrene–Galv system.

3.5. Determination of $|P_n^{DP}|$ and $|P_n^{QP}|$ in coronene– and pyrene–Galv systems

Fig. 6 shows a CIDEP time profile in a coronene–Galv system obtained by monitoring FID intensity as a function of delay time between laser and MW pulses.

Experimental and simulated time profiles are plotted by solid and broken lines, respectively. Contrary to the time profile in a coronene–TEMPO system, the CIDEP signal of $R^{\#}$ created in a S_1–radical encounter seems extremely weak in the overall CIDEP signal. As already discussed in a coronene–TEMPO system (Fig. 4a), both signals of S_1– and T_1–radical systems could appear because a coronene has a relatively long S_1 lifetime of 120 ns and there should be a large number of S_1–radical encounter for CIDEP creation. This observation means the spin polarization in coronene–Galv system due to the S_1–radical encounter is much lower than that due to the T_1–radical encounter, namely $|P_n^{DP}| \ll |P_n^{QP}|$. To discuss this point more quantitatively, we performed simulation of the time profiles on the basis of Bloch Eq. (7) and kinetic Eqs. (8) and (9). Using the kinetic constants listed in Table 2, we simulated the time profile with a parameter of $|P_n^{QP}/P_n^{DP}|$. The ratio of $|P_n^{QP}/P_n^{DP}|$ was changed until the good agreement between simulation and experiment was obtained. The best agreement was obtained with the ratio, $|P_n^{QP}/P_n^{DP}|$ = ca. 9. The simulations with other values such as $|P_n^{QP}/P_n^{DP}| = 4$ and 14 do not reproduce the observed time profile as shown in the figure. The $|P_n^{QP}|$ and $|P_n^{DP}|$ values in a coronene–Galv system were thus determined to be $7P_{eq}$ and $\sim 0.8P_{eq}$ in the unit of P_{eq}. In the same manner, $|P_n^{QP}/P_n^{DP}|$, $|P_n^{DP}|$, and $|P_n^{QP}|$ values in a pyrene–Galv system were determined to be ca. 10, $0.2P_{eq}$, and $2P_{eq}$, respectively. These values are summarized in Table 3.

Table 3
Experimental and calculated values of spin polarizations, $|P_n^{QP}|$ and $|P_n^{DP}|$ in coronene–Galv and pyrene–Galv systems in toluene

	Experiment			Calculation	
	$\lvert P_n^{QP}\rvert$	$\lvert P_n^{DP}\rvert$	$\lvert P_n^{QP}/P_n^{DP}\rvert$	$\lvert^{s}P_n^{QP}\rvert$	$\lvert^{w}P_n^{QP}\rvert$
Coronene–Galv	$(7\pm2)P_{eq}$	$0.8P_{eq}$	9	$(3–9)P_{eq}$	$(0.2–0.6)P_{eq}$
Pyrene–Galv	$(2\pm0.5)P_{eq}$	$0.2P_{eq}$	10	$(3–10)P_{eq}$	$(0.2–0.7)P_{eq}$

The $|P_n^{QP}/P_n^{DP}|$ ratio of ca. 9 for a coronene–Galv system is larger than the ratio of 1.2 for a coronene–TEMPO system. Even though the excited molecules are the same, the spin polarization ratio is found strongly to depend on radical employed.

3.6. Model calculation of $|P_n^{QP}|$

The spin polarization is deeply related to intermolecular potentials and spin dynamics of a radical-excited molecule encounter complex. The spin polarization ($|P_n^{QP}|$) was calculated on the basis of theoretical model proposed by Shushin [7a]. Shushin derived the formulas of the spin polarization for two limiting cases. Judging from the relative energy of exchange interaction (J) and Zeeman energy (ω_0), the strong and weak exchange cases are defined as $|3J_0| \gg \omega_0$ and $|3J_0| \ll \omega_0$, respectively. For the strong exchange case CIDEP is efficiently created on a radical, while for the weak exchange case CIDEP is not. Then, the $|P_n^{QP}|$ value for a strong exchange case is expressed as:

$$|^{s}P_n^{QP}| = \frac{\pi}{45}\frac{D_{zfs}^2}{\omega^2}\frac{\omega_0 d}{\alpha D_r}\left(\frac{1}{1+x^2}+\frac{4}{4+x^2}\right)\frac{d}{r_{QP}} \quad (11)$$

and for a weak exchange case:

$$|^{w}P_n^{QP}| = \frac{8}{45}\frac{D_{zfs}^2}{\omega^2}\frac{|3J_0|dx}{\alpha D_r}\left(\frac{1}{(1+x^2)^2}+\frac{4}{(4+x^2)^2}\right)\frac{d}{r_{QP}} \quad (12)$$

where $x = 1/\omega_0\tau_r$ and τ_r is rotational correlation time. To examine which case is suitable for description of coronene– and pyrene–Galv systems, each $|P_n^{QP}|$ value was calculated by using both Eqs. (11) and (12). For calculation of $|^{s}P_n^{QP}|$ and $|^{w}P_n^{QP}|$ values, the following constants were employed. The ω_0 value is 6.0×10^{10} rad/s under our experimental conditions. Effective diffusion constants (D_r) were obtained using the indi-

vidual D_r values of coronene (2.4×10^{-5} cm^2/s [18]), Galv (1.7×10^{-5} cm^2/s for phenanthrene was adopted [19]), and pyrene (1.7×10^{-5} cm^2/s for phenanthrene was adopted [19]). The individual values were modified based on solvent's viscosity. The resultant D_r values of coronene– and pyrene–Galv pairs are 4.1×10^{-5} and 3.4×10^{-5} cm^2/s, respectively. The rotational correlation time (τ_r) of coronene was estimated to be 10 ps by introducing the D_r value of 1.7×10^{-5} cm^2/s into Stokes–Einstein–Debye equation. The exchange interaction (J) value is expressed as a function of intermolecular distance (r) as:

$$J(r) = 3J_0 \exp\{-\alpha(r - d)\} \tag{13}$$

where d is a distance at the closest approach of an excited molecule and a radical pair, and normally assumed to be 7 Å. The absolute value of $|3J_0|$ used in a weak exchange case is 5×10^9 rad/s [9]. The r_{QP} value, at which a triplet molecule is quenched by a radical, is normally assumed to be equal to the d of 7 Å. The α values were assumed to be from 0.8 to 2.5 Å^{-1} for both coronene– and pyrene–Galv systems, which are typical values on radical–triplet intermolecular potentials [9,16,20]. Zero-magnetic field splitting values (D_{zfs}) of coronene and pyrene are 0.0971 [15] and 0.0929 cm^{-1} [15], respectively.

By introducing all the values into Eqs. (11) and (12), the spin polarizations were calculated as $|^{s}P_n^{QP}| = (3 \sim 9)P_{eq}$ and $|^{w}P_n^{QP}| = (0.2 \sim 0.6)P_{eq}$ for a coronene–Galv system, and $|^{s}P_n^{QP}| = (3 \sim 10)P_{eq}$ and $|^{w}P_n^{QP}| = (0.2 \sim 0.7)P_{eq}$ for a pyrene–Galv system. The results are summarized in Table 3. The experimental $|P_n^{QP}|$ values in both coronene– and pyrene–Galv systems are close to the $|^{s}P_n^{QP}|$ values calculated for the strong exchange case. Therefore, we conclude that the coronene– and pyrene–Galv systems belong to a strong exchange case in the electronic quenching: exchange interaction is much larger than Zeeman energy and CIDEP is efficiently created in coronene– and pyrene–Galv systems.

3.7. Model calculation of r_{DP}

We consider the spin polarization due to S_1–T_1 EISC ($|P_n^{DP}|$) in coronene– and pyrene–Galv systems. The experimentally determined $|P_n^{DP}|$ value is much smaller than the $|P_n^{QP}|$ value for a coronene–Galv system as shown in Table 3. The CIDEP creation mechanism in these electronic quenching processes [9] is explained by spin dynamics on the intermolecular potentials of coronene–Galv pair shown in Fig. 7.

A sign of J value is positive. The symbol of $|^{s}D\ m\rangle$ stands for a doublet spin sublevel built by a singlet molecule and a radical, where m is a magnetic quantum number of +1/2 or −1/2. $|Q\ m\rangle$ and $|D\ m\rangle$ are quartet and doublet spin sublevels, respectively, built by an encounter pair of a triplet molecule and a radical, where m is a magnetic quantum number of +3/2, +1/2, −1/2, or −3/2. The $|Q\ m\rangle$ and $|D\ m\rangle$ sublevels cross each other at the distances of r_c and r_c'. Quenching of singlet and triplet excited molecules by a radical occur at the distances of r_{DP} and r_{QP}, respectively. In a coronene–Galv system, the excited S_1– and T_1–radical pair potentials lie at ∼280 and ∼230 kJ/mol,

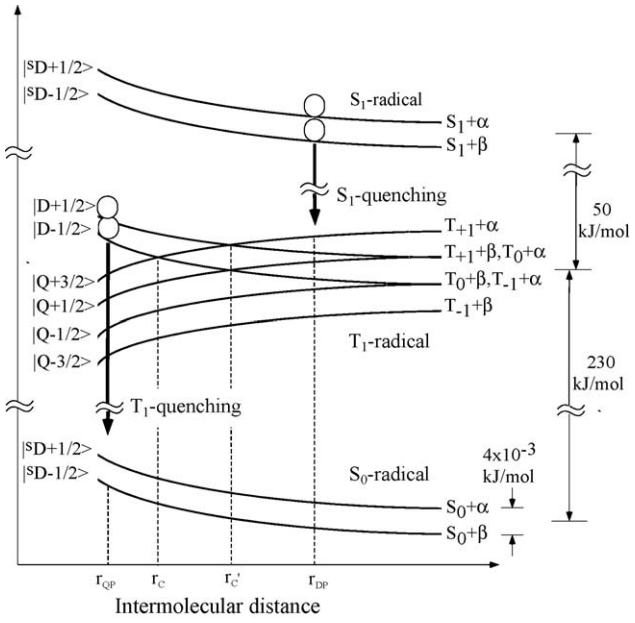

Fig. 7. Schematic diagram to present overall quenching processes and intermolecular potentials. The r_c and r_c' are intermolecular distances at the level crossings. The r_{DP} and r_{QP} are intermolecular distances, around which S_1 and T_1 excited coronenes are quenched by Galv, respectively.

respectively, above the ground S_0–radical potential. The Zeeman splittings between the spin sublevels are negligibly small as 4×10^{-3} kJ/mol. It might be of note that electron spin polarization is created through the nonadiabatic transitions between the nearly-degenerated spin sublevels, which occur around a level crossing region on the T_1–radical pair potentials; $|Q\ +3/2\rangle$, $|Q\ +1/2\rangle$, $|D\ +1/2\rangle$, and $|D\ -1/2\rangle$. As seen in Fig. 7, the level crossings occur at r_c for $|Q\ +3/2\rangle - |D\ -1/2\rangle$ pair, and r_c' for $|Q\ +1/2\rangle - |D\ -1/2\rangle$ and $|Q\ +3/2\rangle - |D\ +1/2\rangle$ pairs.

In general, CIDEP is efficiently created when an excited molecule is quenched around the level crossing distances (r_c or r_c'), while CIDEP is inefficiently created when the quenching occurs at long distance and far from the crossing region. Thus, spin polarization strongly depends on quenching distance. The $|P_n^{QP}|$ value in the T_1–S_0 EISC for a coronene–Galv system is expressed by Eq. (11). The $|P_n^{DP}|$ value in the S_1–T_1 EISC is described by the following Eq. (14) corresponding to the strong exchange case, since exchange interactions in S_1– and T_1–radical encounters occur on the same T_1–radical pair potential of the strong exchange case.

$$|P_n^{DP}| = \frac{\pi}{45}\frac{D^2}{\omega^2}\frac{\omega_0 d}{\alpha D_r}\left(\frac{1}{1+x^2} + \frac{4}{4+x^2}\right)\frac{d}{r_{DP}} \tag{14}$$

Eqs. (11) and (14) are functions of quenching distances, r_{QP} and r_{DP}, respectively. From the combination of Eqs. (11) and (14), Eq. (15) is obtained as:

$$r_{DP} = \left|\frac{P_n^{QP}}{P_n^{DP}}\right| r_{QP} \tag{15}$$

The r_{QP} value of 7 Å which is the closest approach of the pair is normally assumed because T_1-quenching is slightly slower than the diffusion-controlled rate and the contact of the pair

is required [9]. Then, the r_{DP} value of 8.4 Å was estimated for a coronene–TEMPO system [9]. The r_{DP} value is nearly equal to the r_c (=7.8 Å) and r'_c (=8.1 Å) values and though to be reasonable distances. The r_{DP} values for coronene– and pyrene–Galv systems were calculated in the same manner. The r_{DP} values for coronene– and pyrene–Galv systems were estimated to be as large as ~63 and ~70 Å from the experimental values of $|P_n^{QP}/P_n^{DP}|$. These r_{DP} values are apparently too long to be accepted. Because the k_{EISC} values listed in Table 2 are close to a diffusion-controlled rate constant, $1.1 \times 10^{10}\,M^{-1}\,s^{-1}$ (toluene, 20 °C) [15], which means that the S_1–T_1 EISC takes place upon almost every encounter. It is interesting to note that efficient S_1–T_1 EISC does not result in efficient CIDEP generation. The estimation of abnormally large r_{DP} (60–70 Å) seems to indicate that the present quantitative CIDEP theory for the S_1-quenching cannot be applied to the coronene– and pyrene–Galv systems. This limitation of the CIDEP theory may be related to S_1-quenching distance, r_{DP} and thus, we estimated the values for coronene– and pyrene–Galv systems from the kinetic constants. If we apply a simple diffusion-controlled rate theory and the nonadiabatic transition probabilities for S_1–T_1 and T_1–S_0 EISC processes, the rate constants are expressed as [15]:

$$k_{EISC} = 4\pi N_A r_{DP} D_r 10^3 \tag{16}$$

$$k_q^T = 4\pi N_A r_{QP} D_r 10^3 \tag{17}$$

in units of $M^{-1}\,s^{-1}$, where N_A is Avogadro's number. Then, the r_{DP} value is obtained as:

$$r_{DP} \cong \frac{k_{EISC}}{k_q^T} r_{QP} \tag{18}$$

By introducing the k_{EISC}, k_q^T, and r_{QP} (7 Å) values into Eq. (18), we obtain the r_{DP} values of 13 and 9.5 Å for the coronene– and pyrene–Galv systems, respectively. These r_{DP} values might be more reasonable than 63 and 70 Å estimated by Shushin's theory of Eq. (15). It is interesting to note that r_{DP} values of 13 and 9.5 Å are longer than r_c (7.8 Å) and r'_c (8.1 Å) values. For CIDEP creation, efficient quartet–doublet mixings at the level crossing regions are important. The r_{DP} values of 13 and 9.5 Å for coronene– and pyrene–Galv systems mean that the T_1–radical pair produced after S_1–T_1 EISC locates in the region where quartet–doublet mixings are inefficient, namely CIDEP is not created well. This may be why CIDEPs in these S_1–radical systems are very weak, although quantitative calculation of CIDEP has not successfully done yet.

3.8. Electronic quenching mediated by an intermolecular charge transfer state

The above-mentioned discussion leads to a conclusion that r_{DP} in S_1–T_1 EISC is longer than r_{QP} in T_1–S_0 EISC. We discuss the reason below by taking an exemplar coronene–Galv system. The exchange interaction at r_{DP} of 13 Å is much smaller than that at r_{QP} of 7 Å. For faster S_1–T_1 EISC, another quenching mechanism except electron exchange should be considered. If there is additional energy surface between S_1– and T_1–radical pair potentials, additional relaxation pathway from the S_1–radical pair potential will be opened and apparent quenching rate might become faster. The most probable candidate for this unknown intermolecular surface will be a charge transfer (CT) potential [21]. The possibility of the CT contribution is discussed below.

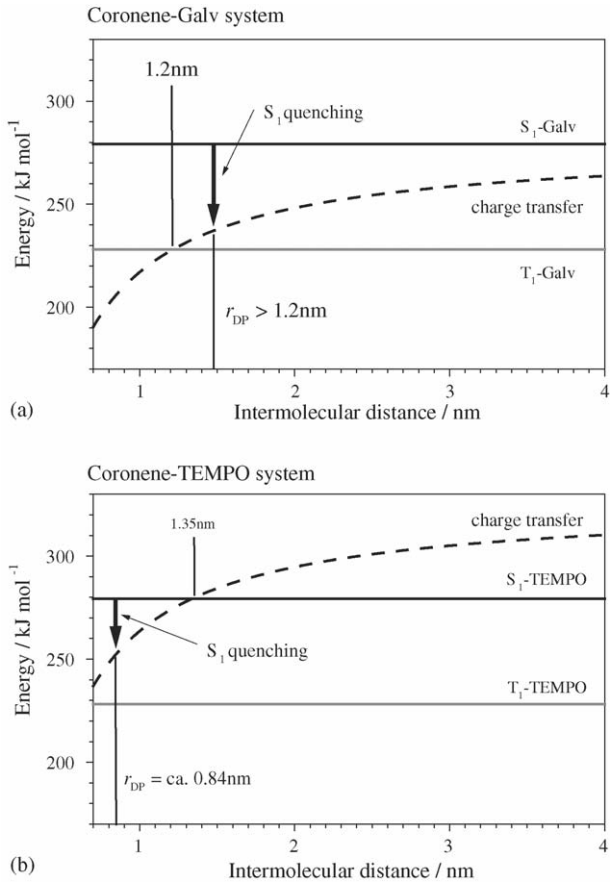

Fig. 8. Model potentials to explain enhanced intersystem crossing from S_1 to T_1 states in coronene. (a) Coronene–Galv and (b) coronene–TEMPO pairs.

The energy of the CT potential ($E_{CT}(r)$) in a coronene–Galv system was estimated as a function of intermolecular distance (r) as:

$$E_{CT}(r) = \{E_{1/2}^{OX}(\text{radical}) - E_{1/2}^{red}(S_0) + \Delta E_{cor}\} + \{\lambda(r) + E_{Coulomb}(r)\} \tag{19}$$

$E_{1/2}^{OX}$(radical) and $E_{1/2}^{red}(S_0)$ mean half-wave redox potentials of radicals and coronene, respectively, versus SCE. The reported values are $E_{1/2}^{OX}(\text{Galv}) = +0.13$ V [22], $E_{1/2}^{OX}(\text{TEMPO}) = +0.63$ V [23], and $E_{1/2}^{red}(\text{coronene}) = -2.07$ V [15]. ΔE_{cor} stands for correction energy and the ΔE_{cor} value of 62 kJ/mol was estimated by using Born equation [22c]. $\lambda(r)$ is solvent reorganization energy in Marcus theory [24] and expressed as $\lambda(r) = \{5.0 - (5.1 \times 10^{-9}/r)\}$ kJ/mol, where we used dielectric constant of 2.379 and refractive index of 1.512. Coulomb energy ($E_{Coulomb}(r)$) is expressed as $-5.9 \times 10^{-8}/r$ kJ/mol. In Fig. 8, we plot the CT energy ($E_{CT}(r)$) using Eq. (19), together with the energies of S_1– and T_1–radical encounter pairs. The S_1- and T_1-excitation energies of coronene are reported to be 280 and 230 kJ/mol, respectively.

As expected, this crude results show CT potential is found to be located below S_1–Galv surface and above the T_1–Galv surface in the intermolecular distance region longer than 12 Å. This means that S_1–T_1 EISC by way of the CT state is exothermic process in coronene–Galv system. The S_1–T_1 EISC occurs possibly through charge transfer interaction in addition to exchange interaction, which results in larger value of r_{DP} than r_{QP}.

Another interesting results is that r_{DP} of coronene–Galv system (13 Å) is longer than that of coronene–TEMPO system (8.4 Å). This is also explained by CT mediated S_1–T_1 EISC mechanism. Fig. 8b shows calculated CT state potential of coronene–TEMPO system. This figure shows that the CT state energy becomes lower than S_1–TEMPO pair energy only when the pair approaches within 13.5 Å. This energy relation suggests that S_1–T_1 EISC can be mediated by both exchange and CT interactions in coronene–Galv system while only by exchange in coronene–TEMPO system when the pairs are at the long distance of more than 13.5 Å. This means that r_{DP} value of coronene–Galv system might be longer than that of coronene–TEMPO system, which agrees with our experimental results.

4. Conclusion

Quenching mechanism of S_1–T_1 and T_1–S_0 EISC processes was investigated by time-resolved fluorescence, thermal lensing, and ESR methods. CIDEP time profiles in coronene– and pyrene–Galv systems were measured by the pulsed ESR method and analyzed to determine spin polarization values. The obtained $|P_n^{QP}/P_n^{DP}|$ values for coronene– and pyrene–radical systems depend significantly on the nature of radicals. The value is close to a unity in coronene–TEMPO system as reported previously while is very large in coroene–Galv and pyrene–Galv systems. The large $|P_n^{QP}/P_n^{DP}|$ value of ca. 9 in coroene–Galv system is explained by considering quenching distances for S_1–T_1 and T_1–S_0 EISC. The former occurs at relatively long distance of 13 Å while the latter occurs at short distance of 7 Å based on theoretical analysis and quenching rate constants. This long distance quenching in S_1–Galv encounter results in less efficient CIDEP creation in S_1–T_1 EISC. According to the estimated intermolecular CT state energy in coronene–Galv encounter pair, the long distance quenching in S_1–Galv encounter was reasonably explained by CT mediated S_1–T_1 EISC in addition to electron exchange mechanism.

Acknowledgements

A.K. and H.T. would like to thank Dr. Keishi Ohara at Ehime University for provision of technical information of synthesis. ESR spectra were measured by one of on-campus cooperative research facilities in Tokyo Institute of Technology, ‘a pulsed EPR system’. This work was partially supported by Grants-in-Aid for Scientific Research (Nos. 17350005 and 15550005) from the Ministry of Education, Culture, Sports, Science, and Technology, Japan.

References

[1] (a) O.L.J. Gijzeman, F. Kaufman, G. Porter, J. Chem. Soc. 69 (1973) 727–737;
(b) O.L.J. Gijzeman, F. Kaufman, G. Porter, J. Chem. Soc. 69 (1973) 708.
[2] (a) A.R. Watkins, Chem. Phys. Lett. 29 (1974) 526;
(b) V.A. Kuzmin, A.S. Tatikolov, Chem. Phys. Lett. 51 (1977) 45;
(c) A.R. Watkins, Chem. Phys. Lett. 70 (1980) 262.
[3] T. Imamura, O. Onitsuka, K. Obi, J. Phys. Chem. 90 (1986) 6741.
[4] C. Blättler, F. Jent, H. Paul, Chem. Phys. Lett. 166 (1990) 375.
[5] (a) A. Kawai, T. Okutsu, K. Obi, J. Phys. Chem. 95 (1991) 9130;
(b) A. Kawai, K. Obi, Res. Chem. Intermed. 19 (1993) 866;
(c) A. Kawai, T. Okutsu, K. Obi, J. Phys. Chem. 96 (1992) 5701.
[6] (a) A. Kawai, K. Obi, J. Phys. Chem. 96 (1992) 52;
(b) Y. Kobori, A. Kawai, K. Obi, J. Phys. Chem. 98 (1994) 6425.
[7] (a) A.I. Shushin, Chem. Phys. Lett. 208 (1993) 173;
(b) A.I. Shushin, Z. Phys. Chem. 182 (1993) 9.
[8] (a) F.J. Adrian, Chem. Phys. Lett. 229 (1994) 465;
(b) A. Blank, H. Levanon, Mol. Phys. 100 (2002) 1477.
[9] M. Mitsui, Y. Kobori, A. Kawai, K. Obi, J. Phys. Chem. A 108 (2004) 524.
[10] R. Kuhn, H. Trischmann, Monatsh. Chem. 95 (1964) 457.
[11] O.M. Polumbrik, Russ. Chem. Rev. 47 (1978) 767.
[12] S. Tero-Kubota, J. Spectrosc. Soc. Jpn. 43 (1994) 266.
[13] T. Suzuki, Y. Kajii, K. Shibuya, K. Obi, Res. Chem. Intermed. 15 (1991) 261.
[14] Y. Kajii, M. Fujita, H. Hiratsuka, K. Obi, Y. Mori, I. Takana, J. Phys. Chem. 91 (1987) 2791.
[15] S.L. Murov, I. Carmichael, G.L. Hug, Handbook of Photochemistry, second ed., Marcel Dekker, New York, 1993.
[16] A. Kawai, K. Shibuya, in preparation.
[17] T. Suzuki, K. Obi, Chem. Phys. Lett. 246 (1995) 130.
[18] V. Hejtmanek, P. Schneider, J. Chem. Eng. Data 38 (1993) 407.
[19] P.L. Bidlack, T.K. Kett, C.M. Kelley, D.K. Anderson, J. Chem. Eng. Data 14 (1969) 342.
[20] (a) G.H. Goudsmit, H. Paul, A.I. Shushin, J. Phys. Chem. 97 (1993) 13243;
(b) Y. Kobori, K. Takeda, K. Tsuji, A. Kawai, K. Obi, J. Phys. Chem. A 102 (1998) 5160;
(c) A.I. Shushin, Chem. Phys. Lett. 313 (1999) 246;
(d) A. Blank, H. Levanon, J. Phys. Chem. A 105 (2001) 4799;
(e) M. Mitsui, K. Takeda, Y. Kobori, A. Kawai, K. Obi, J. Phys. Chem. A 108 (2004) 1120.
[21] (a) A. Kawai, Y. Watanabe, K. Shibuya, Chem. Phys. Lett. 372 (2003) 8;
(b) A. Kawai, K. Shibuya, K. Obi, Appl. Magn. Reson. 18 (2000) 343;
(c) A. Kawai, K. Shibuya, J. Phys. Chem. A 106 (2002) 12305.
[22] A. Samanta, K. Bhattacharyya, P.K. Das, V. Prashant, D. Weir, G.L. Hug, J. Phys. Chem. 93 (1989) 3651.
[23] V.D. Pokhodenko, E.P. Platnova, Soc. Electrochem. 10 (1974) 753.
[24] R.A. Marcus, J. Chem. Phys. 24 (1956) 966.